High Frame-rate TCSPC-FLIM Using a Novel SPAD-based Image Sensor

M. Gersbach[a], R. Trimananda[b], Y. Maruyama[b], M. Fishburn[b], D. Stoppa[c], J. Richardson[d], R. Walker[d,e], R. K. Henderson[e], and E. Charbon[*b]

[a]EPFL, 1015 Lausanne, Switzerland
[b]Delft University of Technology, Mekelweg 4, 2628 CD Delft, Netherlands
[c]Fondazione Bruno Kessler, via Sommarive 18, 38123 Povo, Trento, Italy
[d]STMicroelectronics, 33 Pinkhill, EH12 7BF Edinburgh, Scotland
[e]University of Edinburgh, The King's Buildings, EH9 3JL Edinburgh , Scotland

ABSTRACT

Imaging techniques based on time-correlated single photon counting (TCSPC), such as fluorescence lifetime imaging microscopy (FLIM), rely on fast single-photon detectors as well as timing electronics in the form of time-to-digital or time-to-analog converters. Conventional systems rely on stand-alone or small arrays (up to 32) of detectors and external timing and memory modules. We recently developed a fully integrated image sensor containing 32x32 pixels and fabricated in a 130 nm CMOS technology. The chip produces an overall data rate of 10Gb/s in terms of time-of-arrival measurements in each pixel. As opposed to conventional single detector FLIM systems, the present system can acquire a full image, albeit at low resolution, without the need of an optical scanning system. As a consequence the complexity of the optical setup is reduced and the acquisition speed is dramatically increased. We show the potential of this new technology by presenting high time resolution (119 ps) TCSPC-FLIM images of pollen grains with acquisition times as low as 69 ms. Furthermore, the low noise (~100 Hz) and high photon detection probability (up to 35%) ensure a good photon economy over the visible spectrum. We believe that this technology will open the way to fast TCSPC-FLIM recordings of transient signals in the bio- and life sciences, such as in neuron signaling.

Keywords: single-photon avalanche diode, avalanche photodiode, complementary metal-oxide semiconductor, SPAD, APD, CMOS, fluorescence lifetime imaging microscopy, FLIM

1. INTRODUCTION

Over the past decades fluorescence has been widely developed as a tool for the bio- and life sciences, it is nowadays a common tool extensively used in fields such as biotechnology, flow cytometry, medical diagnostics, DNA sequencing, forensics, and genetic analysis. Recently, with the development of fast detectors and electronics, an additional temporal dimension has emerged, leading to the appearance of fluorescence lifetime spectroscopy, a time-resolved imaging technique [1]. The measurement of the average fluorescence relaxation time, or fluorescence lifetime, allows probing the local environment of the fluorophores at the molecular level. Quantities such as pH, refractive index, ion or oxygen can be measured in a non-invasive manner and without the need for ratiometric measurements. Thus, in essence, in an image with fluorescence lifetime information the contrast may correspond to quantities as diverse as calcium concentration or a protein interaction such as receptor oligomerisation [2]. The vast palette of fluorophores available make time-resolved imaging a method of choice for many non-invasive investigations applied to live cells and tissues.

[*] e.charbon@tudelft.nl; phone +31 15 278-3667; fax +31 15 278-6190; cas.et.tudelft.nl

Detectors and Imaging Devices: Infrared, Focal Plane, Single Photon, edited by Eustace L. Dereniak, John P. Hartke, Paul D. LeVan, Randolph E. Longshore, Ashok K. Sood, Manijeh Razeghi, Rengarajan Sudharsanan,
Proc. of SPIE Vol. 7780 · 77801H · © 2010 SPIE · CCC code: 0277-786X/10/$18 · doi: 10.1117/12.860769

1.1 Fluorescence Lifetime Imaging Techniques

The emission of light from any sample, occurring from electronically excited states, is known as luminescence. The two types of luminescence, phosphorescence and fluorescence, are distinguished by the nature of the excited state as well as the fluorescence lifetime, which corresponds to the average time between excitation and relaxation of the excited state. Fluorescence occurs through the excitation of singlet states, the electron in the orbital is paired (by opposite spin) to the second electron in the ground-state orbital. Thus the transition to the ground state is spin allowed, resulting in a much shorter relaxation time in the order of a few nanoseconds. The transition to the ground state involves the emission of a fluorescent photon. The excitation of the singlet states occurs through the absorption of a photon with energy $E_{ex} = h\nu_{ex}$ where h is Planck's constant and ν_{ex} the frequency of the absorbed photon. The microscopy techniques for the observation and quantification of molecules based on their fluorescence lifetime is known as fluorescence lifetime imaging microscopy (FLIM) [3].

Förster resonance energy transfer [4] (FRET) is another mechanism by which the excited fluorophore can return to its ground state, in part, without radiative transition. FRET occurs when the emission spectrum of the fluorescent molecule (donor) is overlapping with the absorption spectrum on another molecule (acceptor). In many cases the acceptor will not emit a fluorescent photon but return to its ground state by non-radiative processes. The radiationless energy transfer is mediated by dipolar interactions between the donor and acceptor molecule. FRET is useful to quantify the energy transfers between non-fluorescent molecules and fluorescent ones, thereby enabling further extension of the spectrum of observable molecules and molecular mechanisms.

Most fluorescence imaging setups use a single-photon excitation scheme, where a unique photon carries enough energy to excite the single ground state of the fluorescent molecule to be detected. The possibility of exciting fluorescence with multiple photons of lower energy was first studied theoretically by Maria Goeppert-Mayer in her doctoral dissertation in 1931 [5]. The concept involves the near-simultaneous transfer of energy from multiple photons (usually two) to the same fluorescent molecule by which the fluorescence is excited. The probability of near-simultaneous photon absorption is extremely low and thus requires a very high photon flux, typically achievable only with femtosecond laser sources. Apart from the possibility of deep-tissue imaging, the most significant advantage of two-photon microscopy is its inherent three dimensional imaging capabilities without pinholes and other components required for example in confocal imaging. The very high photon flux density required for two-photon excitation results in a highly non-linear excitation probability; the expanded laser beam does not carry enough optical power density to excite the fluorescence while the focused beam will excite the fluorescence due to the higher optical power density.

Finally, as most biological tissues strongly scatter light, the assignment of photons to a particular region of the illuminated section of the sample is often impossible. Two-photon microscopy overcomes this common limitation of traditional microscopic systems, including confocal microscopy, by limiting the fluorescent signal generation to a tiny voxel at the focal point. Two-photon and multiphoton excitation has become a popular tool for the life science community [6]. The potential of two-photon excitation in combination with time-resolved microscopy was demonstrated in [7].

1.2 Fluorescence Lifetime Imaging Applications

For decades fluorescence has been a widely used method in cell biology to monitor cell activity or to highlight certain regions of a cell such as the cell membrane or nucleus, but these observations were mainly qualitative. Quantitative measurements were only possible with intensity-based measurements, which are very prone to variations in excitation intensity as well as fluorophore concentration, a parameter that is extremely difficult to precisely control in a living environment. The emergence of FLIM overcame that limitation since the decay fluorescence intensity is uncorrelated with both the excitation light intensity as well as with the fluorophore concentration.

In cell biology, the most common use of FLIM is to detect FRET upon the interaction between the fluorescent molecule and a specific acceptor molecule. The FRET efficiency being proportional to the inverse 6^{th} power of the donor-acceptor distance, it is suited to measure distances in the nanometer range, acting like a "spectroscopic ruler" to probe intermolecular distances on the molecular scale [8]. The information that can be obtained from FRET ranges from intermolecular distances, molecular interactions as well as distributions of molecular and supramolecular components. In FLIM-FRET the donor molecule is the fluorophore of which the lifetime is measured whereas the acceptor molecules can be various species such specific proteins, lipids, enzymes, DNA or RNA [9],[10],[11],[12].

Another widely used application of FLIM is the ratiometric study of free ion distributions within cells. For example calcium concentrations have accurately and non-invasively been measured by using ratiometric probes such as Oregon Green Bapta (-1,-2 and -5) [12],[13], Calcium Green, Fluo-3, or Quin-2, to name a few [14]. Currently heavily researched is the differentiation of cancerous cells with respect to unaffected tissue using FLIM. Most tissues exhibit autofluorescence, a fluorescent signal that can be observed due to the natural presence of endogenous fluorescent molecules. The observation of the autofluorescent signal can, in certain cases, provide sufficient information to distinguish between healthy and cancerous tissue in skin, colon [15], esophagus [16],[17],[18], brain [19],[20],[21], breast, the oral cavity and skin tumors [22],[23],[24].

Finally, FLIM has also been used to detect chemical reactions and to monitor chemical mixing in microfluidic and lab-on-a-chip type devices. Mixing in microfluidic channels was studied quantitatively and in spatially resolved manner in [25],[26]. Many other studies followed showed to this day and the literature on use of FLIM in these cases is extensive.

1.3 Detecting Fluorescence Lifetime in Solid-state Cameras

Solid-state single-photon detectors for time-resolved applications, and in particular FLIM, have existed for decades. A technique often used to optically evaluate lifetime is based on the principle of time-correlated single-photon counting (TCSPC). In TCSPC, the absorption-emission experiment is repeated several times using a pulsed source; the statistics of the measured relaxation time are then collected as a conventional histogram from which lifetime or multiple lifetimes are extracted. Several solid-state detectors exist in various technologies and ranges of operation, from cryogenic to room temperature detectors and the literature on the subject is extensive [1]. Among those solid-state detectors, avalanche photodiodes (APDs) have emerged as the sensor of choice in the last decade. More recently, a class of APDs operating above breakdown, in so-called Geiger mode has emerged. These devices, known as single-photon avalanche diodes (SPADs), are of particular interest due to their amenability to integration in planar silicon processes in combination with conventional digital and analog circuitries. The first SPADs implemented in a planar technology have emerged in the 1980s [27],[28]. However, the introduction of SPADs implementations in conventional CMOS processes [29], has enabled the evolution of these detectors onto smaller and smaller feature sizes, thus rapidly advancing the state-of-the-art of imagers based on SPADs.

A SPAD is essentially a pn junction biased above breakdown; an impinging photon may generate an electro-hole pair that may, in turn, trigger an avalanche through impact ionization based carrier multiplication. An avalanche quenching mechanism is added to the SPAD to prevent the device's destruction upon the development of an avalanche current through it. After quenching, a certain time, called recharge, is necessary to return to the initial state; the combination of quenching and recharge times is known as the SPAD **dead time**. The dead time is important, as it is the main limiting factor to the detection of large photon fluxes, also known as saturation; it is also responsible in part for non-idealities in lifetime detection, such as photon pile-up. **Afterpulsing** [27], another intrinsic effect of SPADs, is responsible for lifetime skewing and it is also related indirectly to dead time. Afterpulsing is a process by which a primary avalanche is followed by other ones unrelated to photons. The physical process underlying afterpulsing has been

thoroughly researched in the literature; an in-depth characterization of this effect can be found in [30],[31], and [32] for the devices described hereafter.

In SPADs, a strong electrical field within the depletion region allows for the avalanche triggering; this field must be uniformly distributed along the junction; any local variations of the field may be detrimental to the device performance. In planar implementations, the edges of the pn junction must be protected, as the standard diode geometry creates a higher electric field in these locations. This leads to premature edge breakdown and does not allow biasing such a diode above its breakdown voltage. To avoid this effect, SPADs are surrounded by a guard ring; it generally consists of a lesser doped region surrounding the active part of the diode thet lowers the electric field at the borders of the diode to avoid premature edge breakdown. Guard rings can also be implemented using ready-made structures in CMOS, such as shallow trench isolations (STIs). Due to the fabrication process, a large number of free carrier genreation-recombination sites are inherently present at the STI interface. If not recombined before reaching the detector's multiplication region, the free carriers generated at these locations may cause a drastic increase in dark counts. As detailed in [30], an effective technique to reduce STI-related noise consists in implanting a high doping gradient at the STI interface, thus drastically reducing the mean free path of the free carriers and, as a consequence, reducing the probability that these carriers reach the SPAD's multiplication region.

Noise in SPADs is characterized in terms of the mean frequency of dark counts, known as **dark count rate** (**DCR**). Figure 1 shows the cross-section of a typical SPAD implemented in a planar CMOS process. The figure also shows a circuit commonly used to achieve quenching and recharge in these devices.

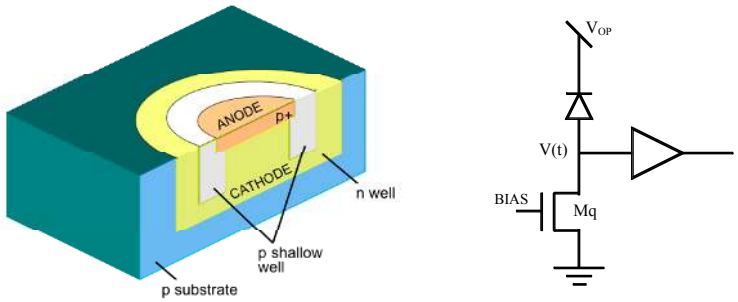

Figure 1. SPAD cross-section in a conventional CMOS process (left); passive quench and recharge circuitries, as well as pulse shaping (right).

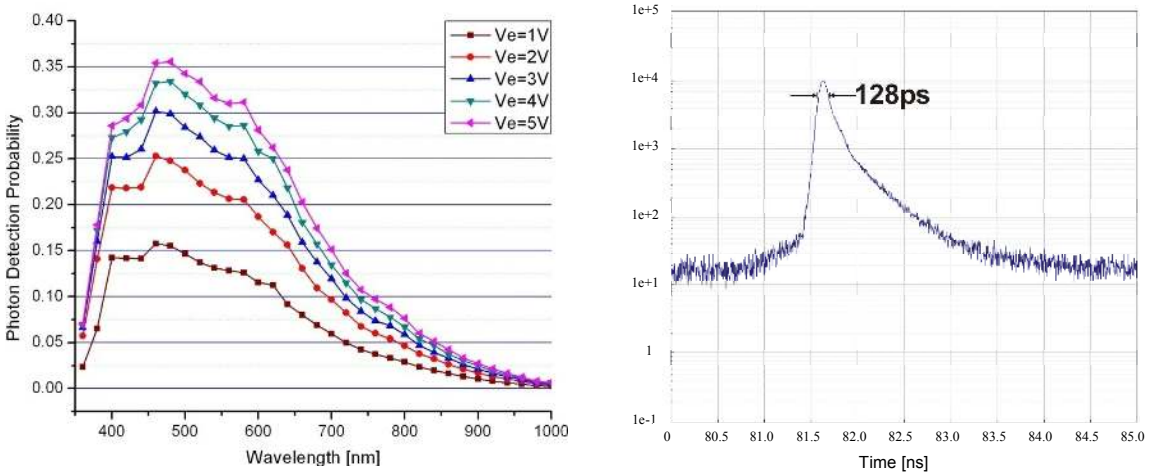

Figure 2. Photon detection probability reported in [30] (left); timing jitter in a130nm CMOS SPAD (right).

The voltage V_{OP} is set so as to present the pn junction with a voltage exceeding the breakdown voltage V_{BD} by a voltage known as excess bias voltage (V_E). There exist a variety of avalanche quenching techniques, partitioned in active and passive methods. In active methods, the avalanche is detected and stopped by acting on the bias. In passive methods the pn junction bias is self-adjusted e.g. by a ballast resistor. The same ballast resistor, often implemented as a biased transistor (M_q in the figure), can be used during the recharge. The resulting dead time can be controlled, to some extent, acting upon the voltage BIAS (also shown in the figure).

Individual SPADs are also characterized by their sensitivity, measured as **photon detection probability** (PDP), and **timing jitter**, or **timing resolution**. These parameters have appeared in the literature for individual SPADs implemented in a variety of CMOS processes [33],[34],[35],[36],[37],[38],[39],[40],[41]. A summary of these performance measures is available in [42]. Figure 2 shows a plot of the PDP as a function of the input wavelength and excess bias voltage in a 130nm CMOS implementation [30]; the figure also reports the timing jitter of the device. A performance analysis of a similar device is reported in [43]. In SPAD arrays, other non-idealities are found, including crosstalk (electrical and optical), PDP non-uniformity, DCR non-uniformity, and timing jitter non-uniformity. [33],[42],[44] report data in all these categories in relation to the architecture selection process for large SPAD arrays.

2. THE MEGAFRAME SENSOR ARCHITECTURE

The goal of the MEGAFRAME project was the design and characterization of a new type of sensor, whereas the target application was FLIM. In the sensor we chose to implement an array of 32x32 pixels amenable to perform TCSPC-FLIM simultaneously and independently. The experiments presented in this paper were achieved using this design that is thus described in some detail hereafter. More details can be found, for this and the other MEGAFRAME architectures in [32],[45],[46].

2.1 Pixel Architecture

Each pixel is equipped with a SPAD and a time-to-digital converter (TDC) capable of computing the time-of-arrival (TOA) of a photon with a resolution of 119ps and a range of 100ns to operate in TCSPC mode. The pixel also includes a 6-bit counter to operate in time-uncorrelated photon counting mode (TUPC).

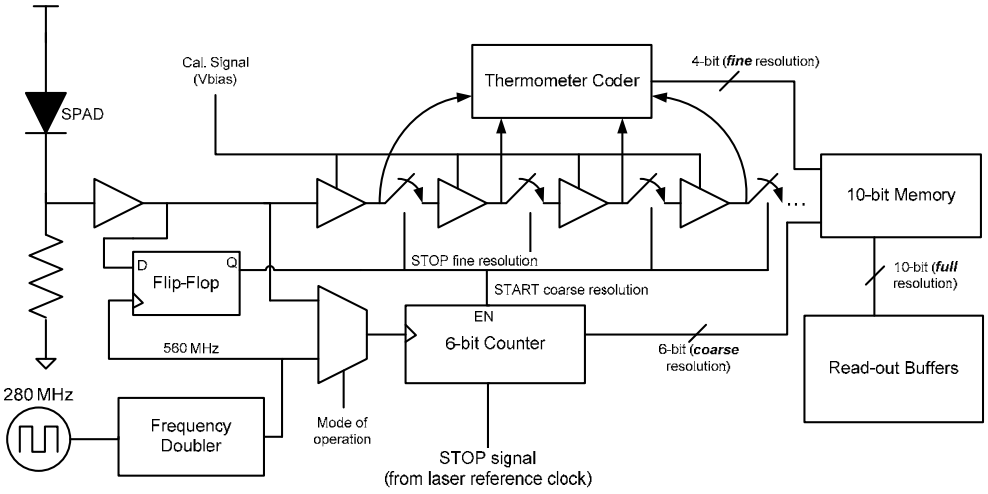

Figure 3. Schematic of the MEGAFRAME pixel. The pixel comprises a SPAD, a 6-bit counter for time-uncorrelated photon counting. The same counter, clocked externally and in combination with a Vernier line, is used to determine the photon time-of-arrival with respect to the reference STOP signal. The Vernier delay line thermometer code is converted to binary in-pixel and read out via the built-in 10-bit memory.

The pixel can generate up to 1Msymbol/s, whereas a symbol may be either a 10-bit binary time code or a 6-bit photon count. The schematic is shown in Figure 3. In TCSPC mode, the SPAD output is used as a START signal, activating the counter that is clocked by a 280MHz signal generated globally by a PLL and doubled on-pixel. This counter determines the coarse photon TOA with respect to the STOP signal with a resolution of 1.8ns. The fine TOA resolution is computed by a 16-element Vernier delay line. The line is frozen by the same clock signal, thus determining the time passing between the START signal and the first subsequent clock rising edge. The thermometer code generated by the Vernier line is converted to binary on-pixel, so as to minimize the lines being read out. The pixel layout is shown in Figure 4. The components of the layout reflect the equivalent components of the schematic described above.

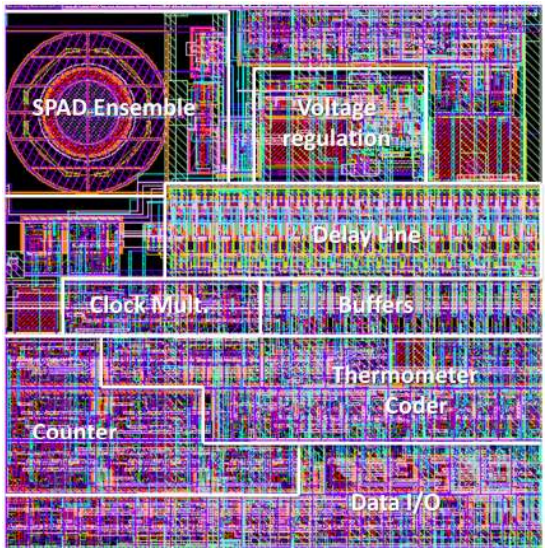

Figure 4. Layout of the pixel implemented in the MEGAFRAME sensor.

The timing diagram of the TDC is shown in Figure 5, whereas the START signal is directly controlled by the SPAD and the STOP signal is synchronized with the clock and it is distributed across the array using a fast H-network.

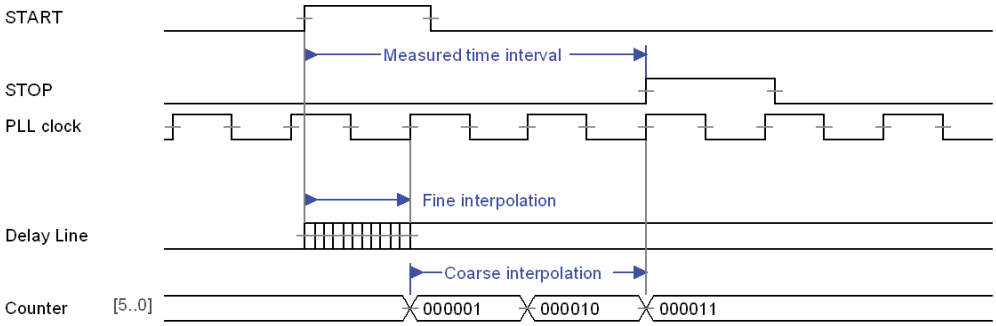

Figure 5. Timing diagram of the time-to-digital converter implemented in the pixel; the SPAD output controls START.

To allow the readout of all 1024 pixels at an overall speed of 1Msymbol/s/pixel, a fast I/O architecture was put in place and implemented using standard cells available in an imaging 130nm CMOS technology provided by STMicroelectronics. The readout of each pixel column is executed sequentially from the top and bottom sides of the sensor in sixteen packets of 10 bits. The I/O pads can achieve a speed of 160Mb/s, thus 64 pads ensure the complete readout of an entire frame, in principle, in 1 microsecond. This frame rate was actually cut in half due to limitations on the external board used to transfer the data to an FPGA. Figure 6 shows the timing diagram of the column readout.

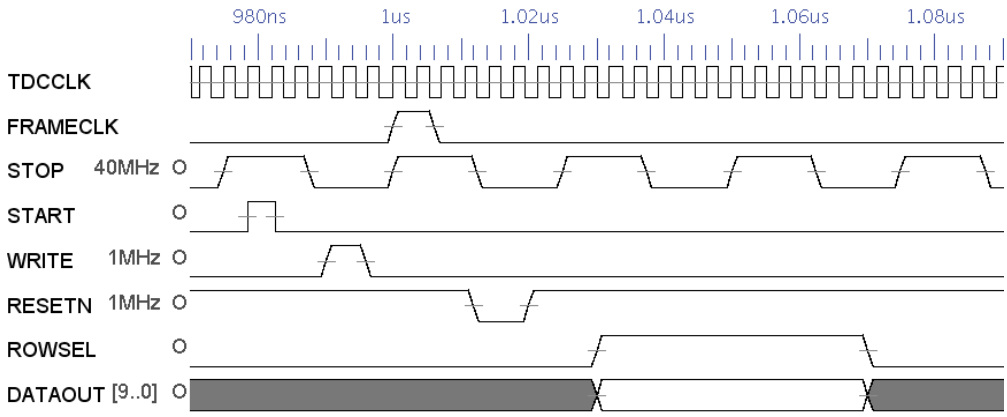

Figure 6. Timing diagram of the column readout scheme used in MEGAFRAME. Note that the STOP signal may be synchronized with a laser synch output signal. Thus the chip may be operating in master or slave mode. The pixel column is read out sequentially in two data paths (top and bottom) each with sixteen 10-bit packets. The readout of the entire frame is completed in 1microsecond.

2.2 Sensor Implementation in CMOS

In order to build large arrays of SPADs, one needs to consider the surroundings of each device. In the MEGAFRAME project, a deep-submicron (DSM) CMOS technology was employed throughout the entire project. It was thus necessary to account for the metals above the device that must be reduced in size and number as much as the technology permits, as they are responsible for significant optical attenuation and undesired reflections

The fill factor in the MEGAFRAME sensors is about 1%. To recover some of the photons impinging outside the SPAD active region, microlenses were implemented on each pixel using the technique outlined in [47]. Figure 7 shows a photomicrograph of the sensor chip (without microlenses). The design includes a phase-lock loop (PLL) frequency synthesizer that generates the clock signals necessary to operate the TDCs. A I^2C block also integrated in the chip manages the various modes of operation seamlessly. More details are reported in [32].

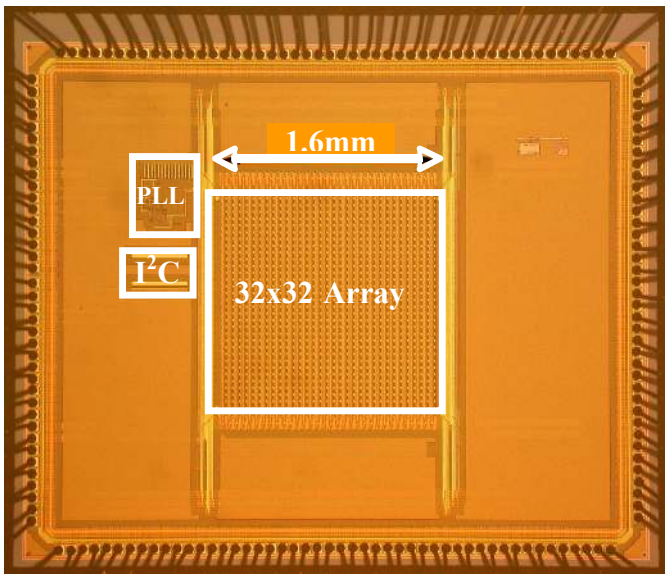

Figure 7. Photomicrograph of the sensor comprising a 32x32 pixel array, capable of performing 1 billion TOA measurements per second with 119ps time resolution.

3. EXPERIMENTAL RESULTS

The MEGAFRAME sensor was completely characterized first in terms of noise and sensitivity. The DCR was computed overall the array and its distribution is plotted in Figure 8. The plot shows a median of less than 100Hz for the array.

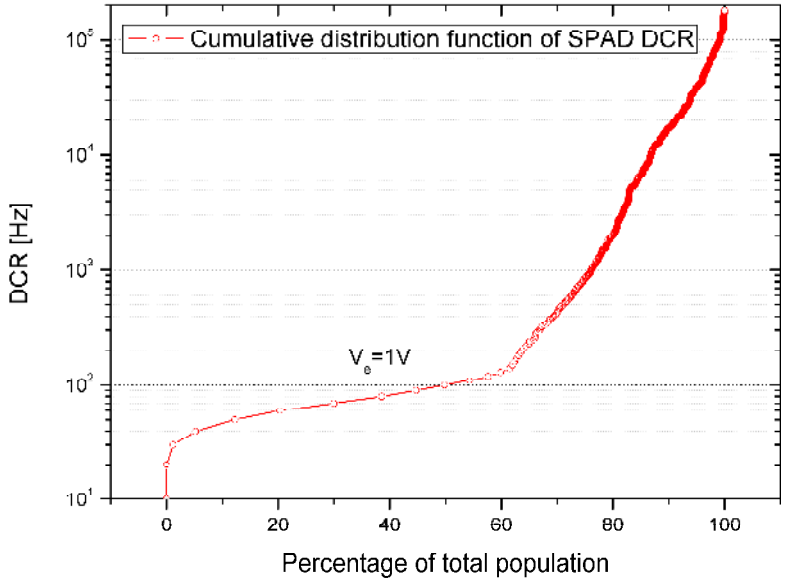

Figure 8. Dark count rate distribution throughout the array at room temperature with an excess bias voltage of 1V.

The TDCs were first characterized in terms of differential and integral non-linearity using the output of the SPAD exposed to continous uniform light as a START signal. The differential and linear non-linearities were thus plotted as a function of the corresponding bins in Figure 9.

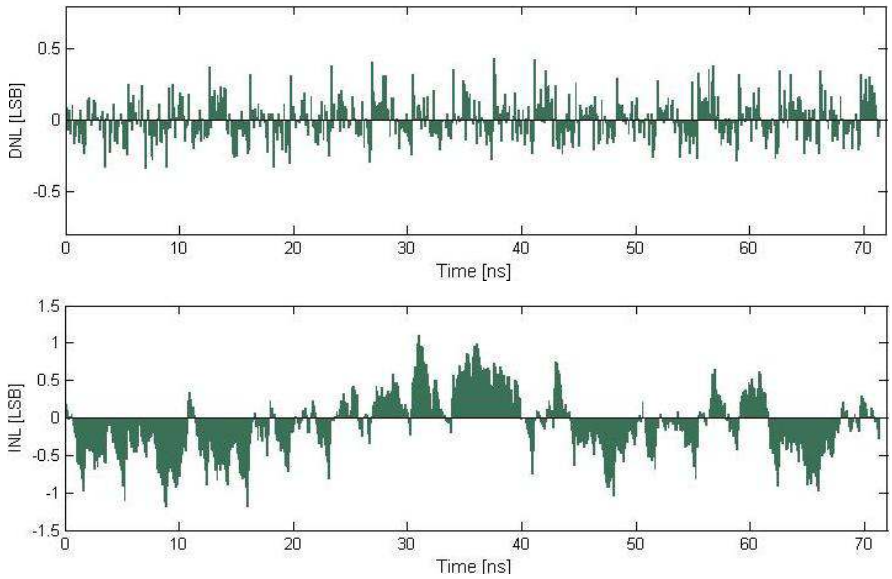

Figure 9. Differential (top) and integral non-linearity (bottom) of the TDC throughout the measurement range.

The timing jitter uniformity is plotted in Figure 10 for all the pixels, whereas a time-domain histogram of the response of a single pixel TDC is also shown in the figure. Overall a jitter uniformity of less than 2LSBs was measured.

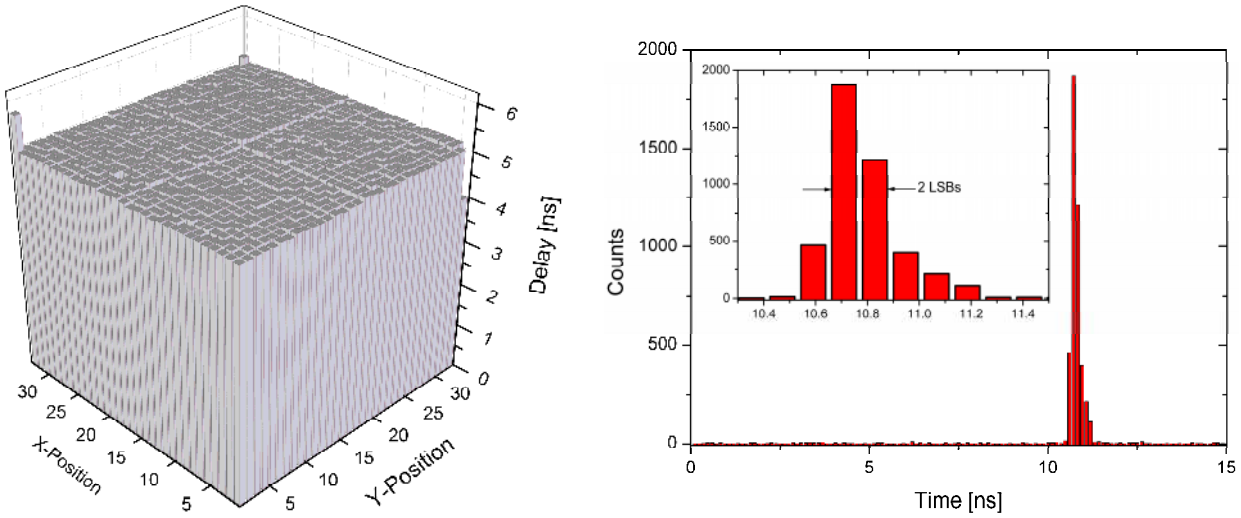

Figure 10. Timing jitter uniformity: FWHM 3D distribution (left), histogram characterization (right).

The table below summarizes the performance of the chip. The overall pixel bandwidth refers to the maximum symbol rate that the image sensor can generate per pixel.

Measurement	Min	Typ	Max	Unit
Format		32x32		-
Fill factor		1		%
Dark count rate at 1V excess (median)		100		Hz
Timing jitter (FWHM)		128		ps
Timing resolution (LSB)		119	111	ps
Differential/integral non-linearity (DNL/INL)		0.4/1.2		LSB
Pixel pitch		50		µm
Overall pixel bandwidth		1,000		kS/s
Count rate			10,000	kc/s
TOA uniformity		2		LSB
Power dissipation (at top speed, without I/O pads)		93.6		mW

The sensor was used in a TCSPC-FLIM electro-optical setup as shown in Figure 11. The imaging setup comprises a pulsed laser source emitting short (<40 ps) light pulses at a frequency of 40 MHz, a wavelength of 405 nm and with an average power of 2 mW (Advanced Laser Diode Systems GmBH, Germany). The laser beam is then directed into a fluorescence microscope (BX51IW, Olympus, Japan) where a dichroic beam splitter cube redirects the beam to the microscope objective (20 x, 0.45 NA, MPlanFL N, Olympus, Japan) and to the sample. The fluorescent light emitted by the sample is captured by the same objective and sent through the dichroic beam splitter, which filters out backscattered laser light, to the SPAD array. The STOP signal is given by the laser's reference signal and the start by the SPADs.

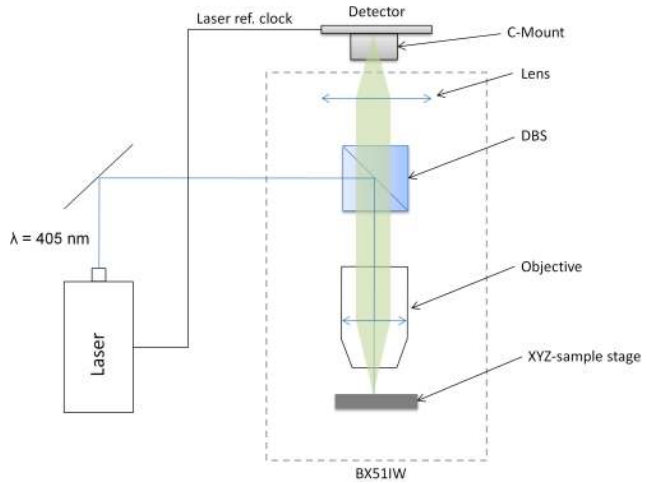

Figure 11. Optical setup of the wide-field TCSPC-FLIM experiment.

The sample used for the wide-field FLIM acquisitions is a mixed pollen grain slide (Carolina Biological Supply Company, NC, USA) containing a mixture of pine, sunflower, cattail, alnus, evening primrose and lily pollen. The pollen grains are stained with either Harris hematoxylin and fast green, or Harris hematoxylin and phloxine. The pollen grain studied in detail in this section is a bisaccate pollen grain of pine stained with Harris hematoxylin and phloxine. The two "sacs" or bladders facilitate wind dispersal of such grains and yield a significant lifetime contrast in the FLIM images. Figure 12 shows the FLIM image of the grain and the corresponding histogram on one pixel obtained using the above setup. The fluorescence lifetime data is collected and stored as an individual histogram for each pixel on the FPGAs present in the readout board. The histograms are then transferred to a personal computer through a USB link. Thanks to the inherent compression rate achieved by the histogramming procedure, near-real-time frame rates are reached. The figure shows how longer exposure times (and slower frame rates) improve the quality of the statistics and thus the accuracy of the extracted lifetime. A quantitative analysis of the results is reported in [48].

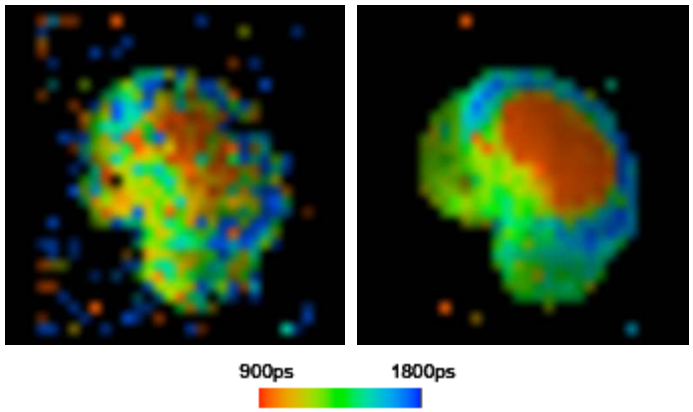

Figure 12. FLIM image of the pollen sample with different exposure times: 69ms (left); 454ms (right).

4. CONCLUSIONS

This paper presents the results from a wide-field FLIM experiment achieved with a new sensor based on an array of SPAD pixels capable of detecting single photons and their time-of-arrival on a pixel-by-pixel basis independently and simultaneously. The sensor is capable of measuring a total of over 1 billion photon arrivals per second with a resolution of 119ps and an integral non-linearity of less than 1.4 LSBs.

Experiments show near-realtime FLIM of pine pollens processed with a two-dye system to enhance certain inner-structures. The whole pollen sample was illuminated by a cone of light without scanning. A FLIM histogram was contructed for each pixel in parallel and used to compress the lifetime data onto the external PC/Mac for display and color assignment. The experiments show the suitability of the approach to obtain high-resolution FLIM images of bio-material and microorganisms without the need of complex optical scanning devices.

ACKNOWLDGEMENTS

This work has been supported by the European Community within the Sixth Framework Programme IST FET Open Megaframe ["Million Frame Per Second, Time-Correlated Single Photon Camera"] project (contract No. 029217-2, www.megaframe.eu).

REFERENCES

[1] E. Charbon, "Will CMOS Imagers Ever Need Ultra-High Speed?", *IEEE International Conference on Solid-State and Integrated-Circuit Technology*, 1975-1980 (2004).
[2] K. Suhling, P.M.W. French, and D. Phillips, "Time-resolved Fluorescence Microscopy," *Photochemical & Photobiological Sciences*, 4, 13-22 (2005).
[3] J.R. Lakowicz, Principles of Fluorescence Spectroscopy, 3rd ed. New York: Springer, 2006.
[4] T. Förster, "Zwischenmolekulare Energiewanderung und Fluoreszenz," *Ann. Phys*., 2(6), 20 (1948).
[5] M. Göppert-Mayer, "Uber Elementarakte mit zwei Quantensprüngen," *Ann. Phys*., 401, 21 (1931).
[6] K. König, "Multiphoton Microscopy in Life Sciences," *Journal of Microscopy*, 200, 83-104 (2000).
[7] P.T.C. So, T. French, W.M. Yu, K.M. Berland, C.Y. Dong, and E. Gratton, "Time-resolved Fluorescence Microscopy using Two-photon Excitation," *Bioimaging*, 3, 49-63 (1995).
[8] L. Stryer and R.P. Haugland, "Energy Transfer - a Spectroscopic Ruler," *Proceedings of the National Academy of Sciences of the United States of America*, 58, 719- (1967).
[9] P.R. Selvin, "The Renaissance of Fluorescence Resonance Energy Transfer," *Nature Structural Biology*, 7, 730-734 (2000).
[10] M. Parsons, B. Vojnovic, and S. Ameer-Beg, "Imaging Protein-protein Interactions in Cell Motility using Fluorescence Resonance Energy Transfer (FRET)," *Biochemical Society Transactions*, 32, 431-433 (2004).
[11] H. Wallrabe and A. Periasamy, "Imaging Protein Molecules using FRET and FLIM Microscopy," *Current Opinion in Biotechnology*, 16, 19-27 (2005).
[12] T.W.J. Gadella, "FRET and FLIM Techniques, "In Laboratory Techniques in Biochemistry and Molecular Biology. 33, S. P. P.C. van der Vliet, Ed.: Elsevier, 542 (2009).
[13] A.V. Agronskaia, L. Tertoolen, and H.C. Gerritsen, "Fast Fluorescence Lifetime Imaging of Calcium in Living Cells," *Journal of Biomedical Optics*, 9, 1230-1237 (2004).
[14] J.R. Lakowicz, H. Szmacinski, W.J. Lederer, M.S. Kirby, M.L. Johnson, and K. Nowaczyk, "Fluorescence Lifetime Imaging of Intracellular Calcium in Cos Cells Using Quin-2," *Cell Calcium*, 15, 7-27 (1994).
[15] M.A. Mycek, K.T. Schomacker, and N.S. Nishioka, "Colonic Polyp Differentiation using Time-resolved Autofluorescence Spectroscopy," *Gastrointestinal Endoscopy*, 48, 390-394 (1998).
[16] R.S. Dacosta, B.C. Wilson, and N.E. Marcon, "New Optical Technologies for Earlier Endoscopic Diagnosis of Premalignant Gastrointestinal Lesions," *Journal of Gastroenterology and Hepatology*, 17, S85-S104 (2002).
[17] T.J. Pfefer, D.Y. Paithankar, J.M. Poneros, K.T. Schomacker, and N.S. Nishioka, "Temporally and Spectrally Resolved Fluorescence Spectroscopy for the Detection of High Grade Dysplasia in Barrett's Esophagus," *Lasers in Surgery and Medicine*, 32, 10-16 (2003).
[18] T. Glanzmann, J. P. Ballini, H. van den Bergh, and G. Wagnieres, "Time-resolved Spectrofluorometer for Clinical Tissue Characterization during Endoscopy," *Review of Scientific Instruments*, 70, 4067-4077 (1999).
[19] L. Marcu, J.A. Jo, P.V. Butte, W.H. Yong, B.K. Pikul, K.L. Black, and R.C. Thompson, "Fluorescence Lifetime Spectroscopy of Glioblastoma Multiforme," *Photochemistry and Photobiology*, 80, 98-103 (2004).
[20] P.V. Butte, B.K. Pikul, A. Hever, W.H. Yong, K.L. Black, and L. Marcu, "Diagnosis of Meningioma by Time-resolved Fluorescence Spectroscopy," *Journal of Biomedical Optics*, 10, 064026 (2005).

[21] J. Leppert, J. Krajewski, S. R. Kantelhardt, S. Schlaffer, N. Petkus, E. Reusche, G. Huttmann, and A. Giese, "Multiphoton Excitation of Autofluorescence for Microscopy of Glioma Tissue," *Neurosurgery*, 58, 759-(2006).
[22] M.C. Skala, K.M. Riching, A. Gendron-Fitzpatrick, J. Eickhoff, K.W. Eliceiri, J.G. White, and N. Ramanujam, "*In vivo* Multiphoton Microscopy of NADH and FAD Redox States, Fluorescence Lifetimes, and Cellular Morphology in Precancerous Epithelia," *Proceedings of the National Academy of Sciences*, 104, 19494-19499 (2007).
[23] H.M. Chen, C.P. Chiang, C. You, T.C. Hsiao, and C.Y. Wang, "Time-resolved Autofluorescence Spectroscopy for Classifying Normal and Premalignant Oral Tissues," *Lasers in Surgery and Medicine*, 37, 37-45 (2005).
[24] B.R. Masters, P. T. So, and E. Gratton, "Multiphoton Excitation Fluorescence Microscopy and Spectroscopy of *in vivo* Human Skin," *Biophysical Journal*, 72, 2405-2412, (1997).
[25] S.W. Magennis, E.M. Graham, and A.C. Jones, "Quantitative Spatial Mapping of Mixing in Microfluidic Systems13," *Angewandte Chemie International Edition*, 44, 6512-6516 (2005).
[26] T. Robinson, P. Valluri, H.B. Manning, D. M. Owen, I. Munro, C. B. Talbot, C. Dunsby, J. F. Eccleston, G. S. Baldwin, M.A.A. Neil, A.J. de Mello, and P.M.W. French, "Three-dimensional Molecular Mapping in a Microfluidic Mixing Device using Fluorescence Lifetime Imaging," *Optics Letters*, 33, 1887-1889 (2008).
[27] S. Cova, A. Longoni, and A. Andreoni, "Towards Picosecond Resolution with Single-Photon Avalanche Diodes", *Rev. Sci. Instr.*, 52(3), 408-412 (1981).
[28] R.J. McIntyre, "Recent Developments in Silicon Avalanche Photodiodes", *Measurement*, 3(4), 146-152 (1985).
[29] A. Rochas *et al*., "Single Photon Detector Fabricated in a Complementary Metal–oxide–semiconductor High-voltage Technology", *Rev. Sci. Instr.*, 74(7), 3263-3270 (2003).
[30] M. Gersbach, J. Richardson, E. Mazaleyrat, S. Hardillier, C. Niclass, R. Henderson, L. Grant, E. Charbon, "A Low-Noise Single-Photon Detector Implemented in a 130 nm CMOS Imaging Process", *Solid-State Electronics*, 53(7), 803-808 (2009).
[31] C. Niclass, M. Sergio, E. Charbon, "A Single Photon Avalanche Diode Array Fabricated in 0.35μm CMOS and based on an Event-Driven Readout for TCSPC Experiments", *SPIE Optics East*, Boston, (2006).
[32] M. Gersbach, Y. Maruyama, E. Labonne, J. Richardson, R. Walker, L. Grant, R. K. Henderson, F. Borghetti, D. Stoppa, E. Charbon, "A Parallel 32x32 Time-to-Digital Converter Array Fabricated in a 130nm Imaging CMOS Technology", *IEEE European Solid-State Device Conference*, (2009).
[33] C. Niclass, A. Rochas, P.A. Besse, and E. Charbon, "Design and Characterization of a CMOS 3-D Image Sensor based on Single Photon Avalanche Diodes", *IEEE Journal of Solid-State Circuits*, 40(9), 1847-1854 (2005).
[34] S. Tisa, F. Zappa, I. Labanca, "On-chip Detection and Counting of Single-photons", *IEEE International Electron Device Meeting*, 815-818 (2005).
[35] C. Niclass, M. Sergio, and E. Charbon, "A Single Photon Avalanche Diode Array Fabricated in Deep-Submicron CMOS Technology", *IEEE Design, Automation & Test in Europe*, 1-6 (2006).
[36] H. Finkelstein, M.J. Hsu and S.C. Esener "STI-bounded single-photon avalanche diode in a deep-submicrometer CMOS technology," *IEEE Electron Device Lett*., 27, 887 (2006).
[37] C. Niclass, M. Gersbach, R.K. Henderson, L. Grant, E. Charbon, "A Single Photon Avalanche Diode Implemented in 130nm CMOS Technology", *IEEE Journal of Selected Topics in Quantum Electronics*, 13(4), 863-869 (2007).
[38] D. Stoppa, L. Pacheri, M. Scandiuzzo, L. Gonzo, G.-F. Della Betta, A. Simoni, "A CMOS 3-D Imager Based on Single Photon Avalanche Diode", *IEEE Trans. on Circuits and Systems*, 54(1), 4-12 (2007).
[39] L. Pancheri and D. Stoppa, "Low-noise CMOS Single-photon Avalanche Diodes with 32ns Dead Time", *IEEE European Solid-State Device Conference*, (2007).
[40] N. Faramarzpour, M.J. Deen, S. Shirani, and Q. Fang, "Fully Integrated Single Photon Avalanche Diode Detector in Standarrd CMOS 0.18-um Technology", *IEEE Trans. on Electron Devices*, 55(3), 760-767 (2008).
[41] C. Niclass, M. Sergio, and E. Charbon, "A CMOS 64x48 Single Photon Avalanche Diode Array with Event-Driven Readout", *IEEE European Solid-State Circuit Conference*, (2006).
[42] E. Charbon, "Single-photon Imaging in CMOS", *SPIE Optics + Photonics*, (2010).

[43] J. Richardson, L. Grant, R. Henderson, "A Low-dark Count Single-photon Avalanche Diode Structure Compatible with Standard Nanometer Scale CMOS Technology", *International Image Sensor Workshop*, (2009).
[44] M.A. Karami, M. Gersbach, E. Charbon, "A New Single-photon Avalanche Diode in 90nm Standard CMOS Technology", *SPIE Optics+Photonics, NanoScience Engineering, Single-Photon Imaging*, (2010).
[45] J. Richardson, R. Walker, L. Grant, D. Stoppa, F. Borghetti, E. Charbon, M. Gersbach, R. K. Henderson, "A 32x32 50ps Resolution 10 bit Time to Digital Converter Array in 130nm CMOS for time Correlated Imaging", *IEEE Custom Integrated Circuits Conference*, (2009).
[46] D. Stoppa, F. Borghetti, J. Richardson, R. Walker, L. Grant, R.K. Henderson, M. Gersbach, E. Charbon, "A 32x32-Pixel Array with In-Pixel Photon Counting and Arrival Time Measurement in the Analog Domain", *IEEE European Solid-State Device Conference*, (2009).
[47] S. Donati, G. Martini, M. Norgia, "Microconcentrators to Recover Fill-factor in Image Photo-detectors with Pixel on-board Processing Circuits", *Opt. Express*, 15, 18066-18074 (2007).
[48] M. Gersbach, "Single-photon Detector Arrays for Time-resolved Fluorescence Imaging", EPFL Thesis N. 4521 (2009).